Experimental Comparison of Cycle Modifications to a Multi-Stage Two-Evaporator Transcritical CO2 Refrigeration Cycle

Riley B. Barta
Purdue University, bartar@purdue.edu

Paige E. Beck

Davide Ziviani

Eckhard A. Groll

Experimental Comparison of Cycle Modifications to a Multi-Stage Two-Evaporator Transcritical CO_2 Refrigeration Cycle

Riley B. BARTA[1*], Paige E. BECK[1], Davide ZIVIANI[1], and Eckhard A. GROLL[1]

[1]Ray W. Herrick Laboratories, School of Mechanical Engineering, Purdue University
West Lafayette, Indiana, 47906, USA
riley.barta@tu-dresden.de; beck128@purdue.edu; dziviani@purdue.edu; groll@purdue.edu

ABSTRACT

With increasing awareness of the adverse effects of carbon emissions on the environment, researchers within the heating, ventilation, air conditioning, and refrigeration (HVAC&R) community have been pushing for lower global warming potential (GWP) and natural working fluids as well as systems that are more efficient than the higher-GWP systems they replace. One such working fluid is carbon dioxide (CO_2). While CO_2 has the advantages of being low-cost, non-flammable, and possessing a high volumetric heat capacity, it has a high critical pressure associated with a low critical temperature, thus often necessitating transcritical operation that requires significant compressor input power. As such, numerous cycle modifications have been proposed that enable the transcritical CO_2 cycle to match, and in some cases surpass, the coefficient of performance (COP) of existing hydrofluorocarbon (HFC) cycles under the same operating conditions. This work provides an experimental comparison of four cycle architectures that utilize the same compressors and heat exchangers. This enables a meaningful comparison of these modifications, consisting of open economization with an evaporator bypass, as well as both electronic expansion valve (EXV) and ejector expansion strategies, along with a pump applied between the gas cooler outlet and the ejector motive nozzle inlet for control and increased recoverable pressure differential. Experimental parametric studies were conducted, and comparisons of architecture costs and benefits are presented. Design recommendations are provided along with future work.

1. INTRODUCTION

Since the revitalization of carbon dioxide (CO_2) as a refrigerant in the 1990s (Lorentzen, 1994), extensive research has been conducted on increasing the efficiency of vapor compression cycles utilizing CO_2 to compete with, and eventually surpass, the efficiencies of hydrofluorocarbon (HFC) cycles. Unique thermo-physical properties of CO_2 were discussed by Kim et al. (Kim et al., 2004), where the intricacies of transcritical operation were identified. In particular, the rejection of heat in the supercritical region decouples temperature and pressure as they become independent, intensive properties outside of the two-phase region, making the heat rejection process gas cooling instead of condensing, resulting in a gas cooling pressure that results in a maximum coefficient of performance (COP) for a given operating condition.

A significant number of cycle modifications have been proposed to improve the COP of transcritical CO_2 cycles, and within this topic expansion work recovery has proven to have significant potential. One of the most widely-used methods of expansion work recovery is an ejector, which was first introduced by Gay (Gay, 1931). The past decades have brought about a large amount of numerical and experimental research on ejectors (Kemper, G.A., Harper, G.F., Brown, 1996; Liu et al., 2012; Lucas and Koehler, 2012; Newton, 1972; Bahman et al., 2021). However, because the primary purpose of an expansion device in a vapor compression cycle is cycle control, active control of the ejector has become a research focus. Elbel and Hrnjak investigated an ejector with a variable-diameter motive nozzle (Elbel and Hrnjak, 2008), resulting in COP and cooling capacity improvements of 7% and 8%, respectively, as well as proving the device control could be used to vary the gas cooling pressure of the cycle to achieve a maximum COP. Another strategy for ejector control is the multi-ejector, introduced by Hafner et al. (Hafner et al., 2014) and experimentally-investigated by Haida et al. (Haida et al., 2016). In the latter work, COP and exergetic efficiency benefits of 7% and 13.7%, respectively, were obtained and cycle stability was validated through variation of both ambient temperature and flash tank pressure. Zhu and Elbel (Zhu and Elbel, 2018) found that introducing a tangential flow upstream of a converging-diverging nozzle to impart a swirl could be an effective method to control nozzle performance. The researchers successfully varied the mass flow rate necessary to achieve choked flow by 42% at the same operating conditions.

Multi-evaporator cycles are commonly applied in both supermarket and transport refrigeration due to the need to maintain cooling compartments at different temperatures while using a central vapor compression cycle. The cycle architectures applied in transcritical CO_2 supermarket applications vary in complexity in order to achieve a performance benefit over the HFC cycles they seek to replace depending on the proposed ambient conditions (Karampour and Sawalha, 2018). On the complex end of this spectrum, Minetto et al. (Minetto et al., 2014) experimentally investigated parallel compression, ejector expansion work recovery, and flooded evaporation in a multi-evaporator architecture, reducing compressor power consumption by 13% at an ambient temperature of 16 °C. Gullo and Hafner (Gullo and Hafner, 2017) assessed several existing supermarket systems and found that first generation booster technology could achieve higher COP values than a direct expansion R-404A system at ambient temperatures up to 14 °C. In contrast, the maximum temperature where the efficiency of an R-404A supermarket refrigeration system is lower than that of a CO_2 system increased to 27 °C with more advanced parallel compression system designs. A summary of the state-of-the-art of supermarket refrigeration cycles can be found in Gullo et al. (Gullo et al., 2018), which provides numerous examples of multi-evaporator architectures, expansion work recovery, and phase separation.

To offer a transportation container refrigeration perspective, Lawrence et al. (Lawrence et al., 2018) numerically assessed the performance of a multi-temperature refrigerated transportation container system using a transcritical CO_2 with an ejector and internal heat exchanger, resulting in a COP of 0.96 at an extreme ambient temperature of 57 °C. Barta et al. (Barta et al., 2018) also investigated a multi-temperature refrigeration container system numerically, applying an expander and a flash tank upstream of the MT evaporator, achieving a COP of 1.28 at an ambient temperature of 57.2 °C. These papers numerically displayed the ability of complex cycles to be applied to multi-evaporator transportation container refrigeration systems in an effort to achieve COP values equal to or over unity, motivating further experimental investigation.

This paper presents a comprehensive experimental comparison of modifications to a multi-stage two-evaporator transcritical CO_2 refrigeration cycle. The multi-stage and open-economization combination with an ejector was informed by Ladd (2018, 2019a, 2019b, 2019c) with the intention of validating a particular multi-stage flashing refrigeration cycle as well as use of a pump to increase the performance of the ejector. Among the cycle comparisons are two methods for ejector control. The first control method is a variable motive nozzle and the second is the addition of a variable-speed pump located at the gas cooler outlet to vary the ejector motive nozzle inlet pressure. The results of a comprehensive comparison parametric study are presented, and both lessons learned and next steps are presented after the discussion of results.

2. SYSTEM OVERVIEW

2.1 Overall Design

The experimental test stand utilized in this work features two evaporation temperatures, three stages of compression, intercooling between the second and third compression stages, a flash tank at the medium-temperature (MT) evaporator inlet, and either an electronic expansion valve (EXV) or an ejector for expansion. An ejector recovers expansion work by accelerating the high-pressure flow from the gas cooler outlet via a motive nozzle into a motive flow which entrains low-pressure flow from the evaporator outlet through a suction nozzle. The two flows then mix and diffuse at a pressure greater than the evaporation pressure, which reduces the amount of pressure lift required of the compressor and thus, reducing the required input power. Open economization is conducted with a flash tank, which is a large vessel that two-phase flow enters and flashes into separate phases as a result of the sudden increase in volume. Gravity then further separates the phases such that the saturated vapor flows out the top of the tank to bypass the evaporator while the saturated liquid exits the bottom of the tank to enter the evaporator at a lower specific enthalpy than the evaporator would receive without phase separation. This can result in an increased cooling capacity if the impact of the larger change in specific enthalpy across the evaporator outweighs the disadvantage of the reduced mass flow rate passed through the evaporator as a result of the vapor bypass.

In the test stand utilized herein, the flow from the outlet of the gas cooler can be directed through an EXV, directly to the ejector motive nozzle inlet, or through a pump before entering the motive nozzle inlet. In the latter two scenarios, the flow from the MT evaporator is routed to the suction nozzle of the ejector instead of to the second stage compressor suction. The ambient conditions are controlled with the psychrometric chamber where the test stand is located, and both evaporators are controlled by independent Ethylene-Glycol (EG) baths. The MT EG-side evaporator inlet temperature target was 3 °C to simulate refrigeration applications, and the low-temperature (LT) EG-side evaporator inlet temperature target was -21 °C to simulate freezer applications. Ambient relative humidity was set at 30% in order to minimize frost formation on the ejector. A piping and instrumentation diagram (P&ID) of the test stand is shown in Figure 1.

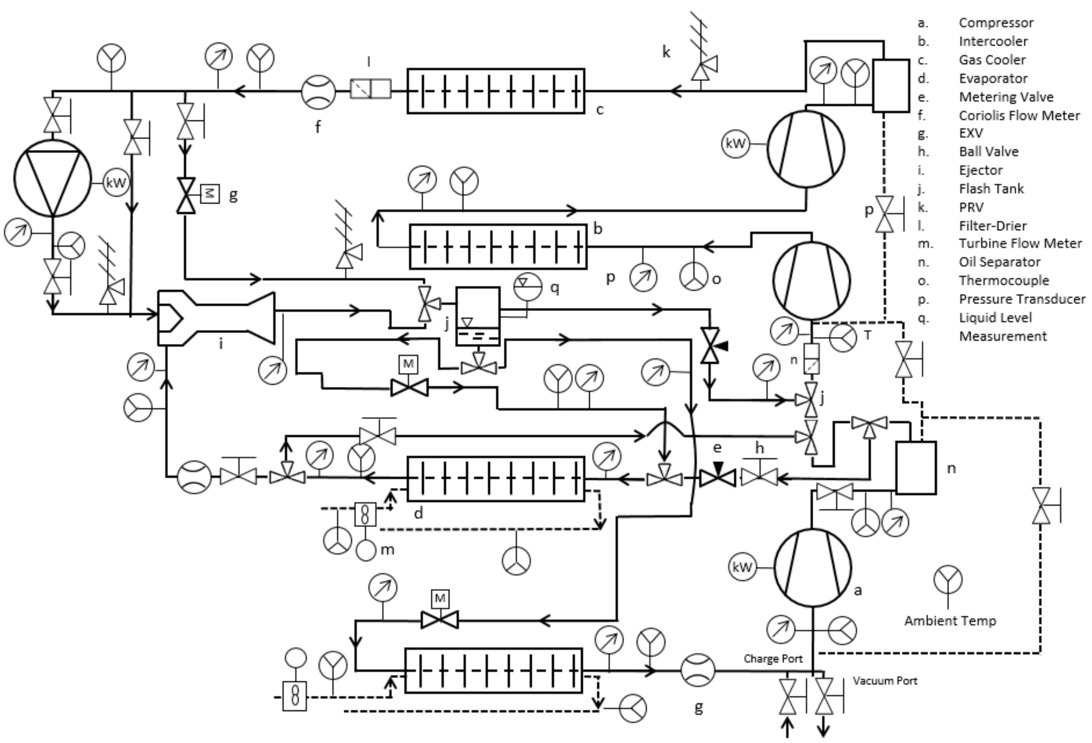

Figure 1: P&ID of the test stand.

2.2 Analyzed Cycles

Four cycle architectures were experimentally investigated over a range of operating conditions. The first cycle was treated as the baseline and consists of isenthalpic expansion through an EXV with no flash tank phase separation. Next, a flash tank was applied upstream of the MT evaporator to facilitate open economization, where saturated vapor is throttled to the evaporator inlet and the vapor bypasses the evaporator. The third cycle utilized an ejector with motive flow from the gas cooler outlet and suction flow from the MT evaporator outlet. The ejector diffuser outlet flow then enters the flash tank where the same economization process from the second cycle occurs. Finally, a pump was added between the gas cooler outlet and the motive nozzle inlet. This was done in order to modulate the motive nozzle input state to provide control of the ejector efficiency, pressure lift, and entrainment ratio, as well as to increase the cycle efficiency by providing additional pressure differential across the motive nozzle, and thus additional potential work for expansion work recovery. The idea behind applying a pump was that it requires less work to increase the pressure of a liquid than a gas due to the smaller change in specific volume for a given pressure rise associated with less-compressible fluid states. Therefore, the work required by the pump would result in an increase in ejector pressure lift, thus decreasing the work input required by the compression process. The ejector utilized in this work was developed and tested in Liu et al. (Liu et al., 2012), and the motive nozzle diameter was varied manually during testing through rotation of a threaded needle with a wrench to move the needle in and out of the motive nozzle throat.

The gas cooler pressure was varied in order to find the pressure that resulted in the maximum COP at each ambient condition, and steady-state results were collected for all four architectures. Ambient temperatures of 14 °C, 19 °C, 24 °C, and 28 °C were assessed for all architectures except the architecture that utilized the pump, which was only tested at 14 °C and 19 °C conditions in order to meet the maximum pump suction temperature restrictions.

2.3 Measurements and Instrumentation

All single-phase states were measured using calibrated in-line thermocouples and pressure transducers. Many two-phase states were assessed with both temperature and pressure for redundancy. Three Coriolis mass flow meters were used to measure refrigerant mass flow rates, and one turbine flow meter was placed in each EG loop. The EG temperature was measured at the inlet and outlet of each evaporator with in-line thermocouples placed in the EG flow. Mass concentrations of 34% and 50% EG were utilized in the MT and LT temperature baths, respectively. Both of the compressors and the pump were controlled with variable frequency drives (VFD), and the power consumption for each device was measured between the power source and the VFD. Fan power for in the intercooler and gas coolers was measured via watt transducer, and an estimated 0.5 kW of fan power for the simulation of the evaporators as air source components was applied based on experimental data from another project with air source evaporators applied in container cooling. The flash tank liquid level was monitored by a sight glass and capacitive liquid level sensors to pass the liquid level signal to the data acquisition as well as for redundancy. The P&ID shown in Figure 1 provides a visual reference for the location of the measurement devices, and details of the various measurements are provided in Table 1.

Table 1: Summary of sensors and corresponding uncertainty.

Physical Parameter	Description	Model	Accuracy
Temperature	Ungrounded TC	Omega T-Type	$\pm$0.5 K
Pressure (HP Side)	PT, 0-20684 kPa	Setra 206	$\pm$26.9 kPa
Pressure (LP Side)	PT, 0-6895 kPa	Setra 206	$\pm$9.0 kPa
Mass Flow ($\dot{m}_{\text{motive}}$)	Coriolis Flow Meter	Micromotion CMFS050	$\pm$0.1% RDG
Mass Flow ($\dot{m}_{\text{suction}}$)	Coriolis Flow Meter	Micromotion F025	$\pm$0.2% RDG
Mass Flow ($\dot{m}_{\text{LT}}$)	Coriolis Flow Meter	Micromotion F025	$\pm$0.2% RDG
Volume Flow ($\dot{V}_{\text{EG}}$)	Turbine Volume Flow Meter	Omega FTB-1424	$\pm$0.1% FS
Liquid Level	Capacitive Liquid Sensor	SWI CS02	$\pm$0.5% Linearity
Compressor Power	Watt Transducer	Ohio Semitronics GW5-015E	$\pm$0.2% RDG $\pm$0.05% FS
Fan Power	Watt Transducer	Ohio Semitronics PC8-001	$\pm$1.0% FS

All of the accuracy of instrumentation are used to determine the uncertainty of independent variables as calculated in Equation 1 from Taylor and Kuyatt (1994).

$$U_{\text{Y}} = \sqrt{\sum \left(\frac{\partial Y}{\partial X_i} U_{x_i}\right)^2} \tag{1}$$

where *Y* is the calculated quantity, *X* is the measured quantity, and *U* is the uncertainty. The COP calculation is shown in Equation 2.

$$COP = \frac{\dot{Q}_{\text{cool,LT}} + \dot{Q}_{\text{cool,MT}}}{\dot{W}_{\text{comp,LP}} + \dot{W}_{\text{comp,HP}} + \dot{W}_{\text{pump}} + \dot{W}_{\text{fans}}} \tag{2}$$

Ejector entrainment ratio, w, and ejector efficiency, η_{ejector}, are given by Equations 3 and 4, respectively.

$$w = \frac{\dot{m}_{\text{suction}}}{\dot{m}_{\text{motive}}} \tag{3}$$

where *suction* refers to the suction nozzle flow and *motive* refers to the motive nozzle flow.

$$\eta_{\text{ejector}} = w \frac{h(s_{\text{si}}, P_{\text{d}}) - h_{\text{si}}}{h_{\text{mi}} - h(P_{\text{d}}, s_{\text{mi}})} \quad [4]$$

where h is specific enthalpy, P is pressure, s is specific entropy, si denotes the suction nozzle inlet, mi denotes the motive nozzle inlet, and d denotes the ejector diffuser outlet. The pressure lift achieved by the ejector is defined as the difference in pressure between the ejector diffuser outlet and the evaporator outlet.

3. PARAMETRIC COMPARISON BETWEEN ARCHITECTURES

The results of this study include 58 steady-state data points consisting of between five and ten minutes of steady measurement for each point. Statistics of parameters concerning the consistency and comparability of the tests are provided in Table 2. A target compressor suction superheat of approximately 13.5 K was chosen because of cycle instabilities that resulted when the evaporator outlet state transitioned from superheated vapor to a high-quality two-phase flow. Charge was held constant at a value of 7.9 kg for all tests utilizing the flash tank. The charge for the baseline tests was between 4.6 kg and 5.1 kg for different ambient conditions to maximize the range of operating conditions that could be achieved due to the lack of charge storage flexibility afforded to the other architectures by the flash tank. Any sub-critical data points had measured sub-cool of at least 1.8 K, and all but two points had sub-cool greater than 4 K. The overall system energy balance was within 6% for all tests, and the EG-side heat transfer rates were taken as the cooling capacity values for both evaporators due to the discovery that two of the three Coriolis mass flow meters in the refrigerant line were not reliable because their placement at the outlet of both evaporators subjected the Coriolis mass flow meters to oil and occasional two-phase flow conditions, rendering their measurement less reliable. Logarithmic pressure-specific enthalpy (P-h) diagrams of each cycle are provided in Figure 2, Figure 3, Figure 4, and Figure 5. The P-h diagrams represent the gas cooling pressure which achieved the highest COP for each ambient condition tested.

Table 2: Statistical parameters on test condition consistency.

Parameter	Average Value	Standard Deviation
LT Evaporator EG Inlet Temperature	-20.7 °C	0.4 °C
MT Evaporator EG Inlet Temperature	2.6 °C	0.7 °C
1st Stage Compressor Suction Superheat	14.4 °C	1.4 °C
2nd Stage Compressor Suction Superheat	13.1 °C	1.5 °C

4. RESULTS AND DISCUSSION

The ejector was originally sized for a 15 kW air conditioning system, and was therefore oversized for the test stand at refrigeration conditions, which had an approximate total capacity of 8 kW. This led to a reduced efficiency, but the motive nozzle was still able to be modulated to provide adequate control of the gas cooling pressure. The pump design maximum inlet temperature is 25 °C in order to retain a sub-cooled or supercritical liquid state of the working fluid. Therefore, it was only applied at the 14 °C and 19 °C ambient conditions. The maximum speed the pump was operated at was limited to a speed that would keep the pump discharge pressure below the maximum design discharge pressure of 100 bar. The second stage compressor proved to be another limiting factor in test stand operation due to being undersized, resulting in the inability to reach a gas cooling pressure corresponding to a maximum COP at the 28 °C condition because of the motor current draw limit.

The high-side EXV was modulated to vary across a range of gas cooling pressures in search of the maximum COP for each cycle and condition that did not employ the ejector, bounded by the aforementioned experimental limitations. Pressures corresponding to the maximum COP were identified at all ambient conditions except the 28 °C condition, and for all cycles except the cycle with the pump. In the case of the pump cycle, the COP value decreased with increasing pump speed for all points tested. The ejector motive nozzle was at the minimum motive diameter for both conditions where the pump was applied in order to minimize the chance of cavitation in the pump suction chamber due to the pump suction state entering the vapor dome. The resulting COP values with gas cooling pressure variation for all four ambient conditions are shown in Figure 6, Figure 7, and Figure 8 for the baseline, MT economization, and ejector cycles, respectively.

The COP trends followed the expected result of attaining a maximum value for a given ambient condition at a higher pressure with increasing ambient temperature. The maximum COP values for each cycle and ambient temperature are plotted at the corresponding gas cooler outlet pressure in Figure 9 for an overall comparison. The two pump points are plotted showing the highest speed tested. This means that the COP values for pump operation range from the value shown in Figure 9 up towards the COP value shown at the highest pressure for the corresponding ambient temperatures with the ejector cycle in Figure 8, which would represent the cycle COP before the pump was engaged.

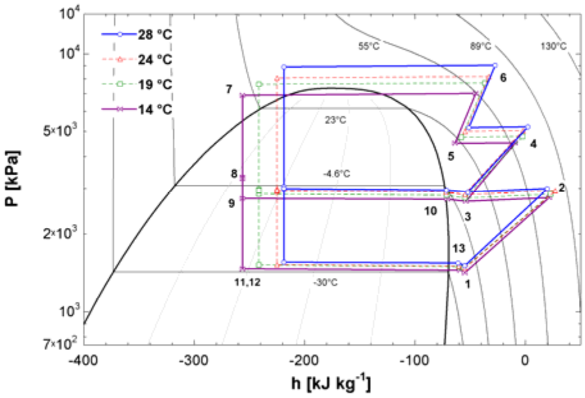

Figure 2: P-h diagram of baseline cycle.

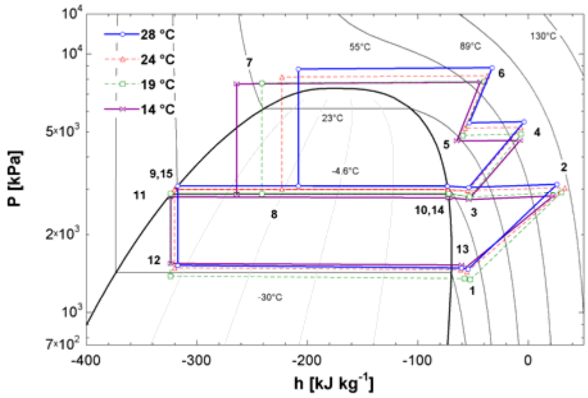

Figure 3: P-h diagram of MT economization cycle.

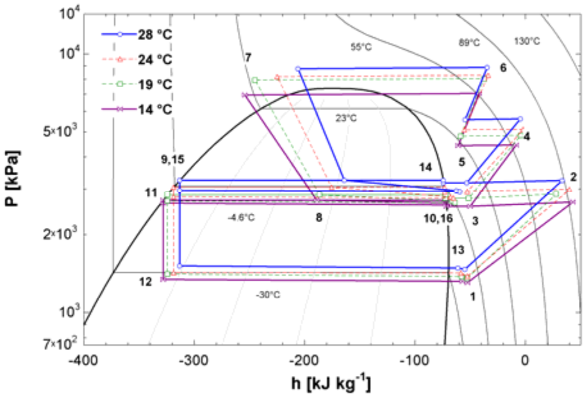

Figure 4: P-h diagram of ejector cycle.

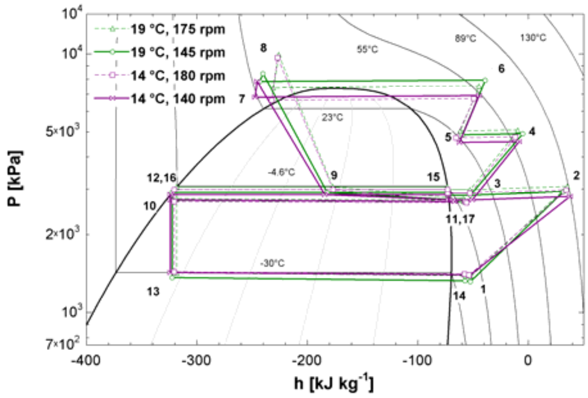

Figure 5: P-h diagram of ejector with pump cycle.

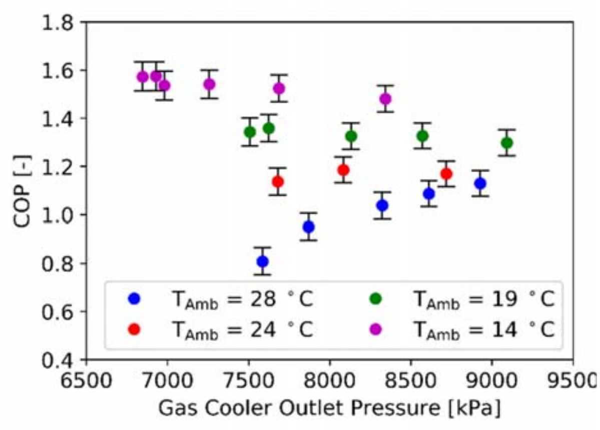

Figure 6: Baseline cycle COP with gas cooling pressure variation.

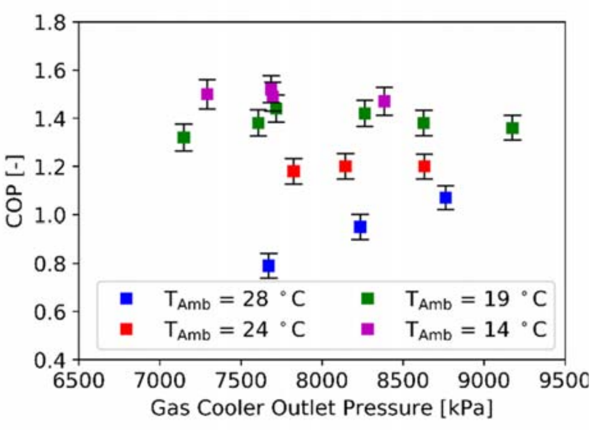

Figure 7: MT economization cycle COP with gas cooling pressure variation.

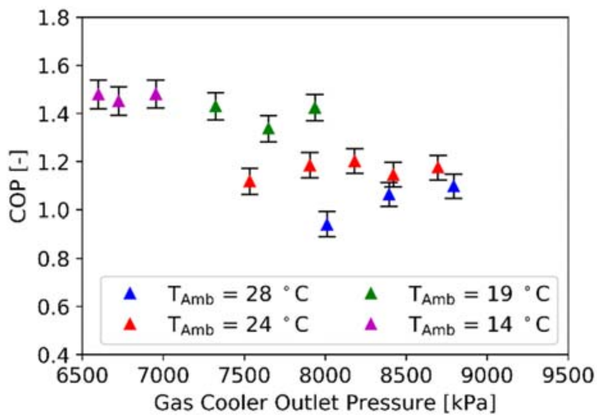

Figure 8: Ejector cycle COP with gas cooling pressure variation.

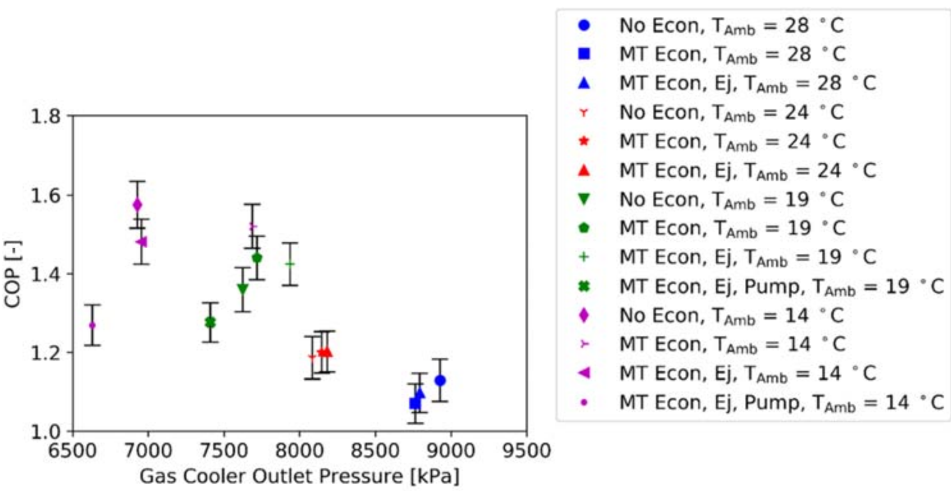

Figure 9: Summary of maximum achieved COP for tested architectures.

Maximum COP improvements of 6% and 5% over baseline were obtained with the MT economization and ejector cycles, respectively, at the 19 °C ambient condition. The lower COP benefit with the ejector cycle relative to the MT economization cycle is largely the result of a lower-efficiency ejector. A reduced ejector lift resulting from lower ejector efficiency did not reduce the compressor power as much as intended, and the higher diffuser outlet quality relative to the flash tank inlet quality observed in the MT economization compounded the effect of the lower ejector pressure lift and resulted in a slightly smaller COP benefit with the ejector cycle. Smaller COP improvements from the MT economization and ejector cycles were obtained at the 24 °C condition. Figure 4 justifies why the ejector COP benefit did not increase with ambient temperature at the 24 °C ambient condition by showing that the ejector motive nozzle inlet pressure does not increase significantly past the cycle shown at the 19 °C ambient condition. The small increase in gas cooling pressure at the 24 °C ambient condition suggests that there may have been a slightly higher pressure that would have optimized the cycle further, despite Figure 8 appearing to have achieved a maximum COP for the 24 °C ambient condition. Both the MT economization and ejector cycles resulted in lower maximum COP values at the 14 °C and 28 °C conditions. The lower COP at the 14 °C condition is largely due to the low evaporator inlet quality achieved with the baseline cycle due to the low condenser outlet temperature. In this case, the benefit of an increased change in specific enthalpy across the evaporator is less significant such that the detrimental effect of the reduced mass flow rate through the evaporator due to phase separation on the cooling capacity outweighed the benefit of the lower evaporator inlet quality. A similar explanation can be given for the decrease in COP of the cycle utilizing the ejector, as the reduction in mass flow rate through the evaporator was not outweighed by the decreased compressor input power required. This is a result of the ejector being unable to increase the compressor suction pressure enough due to a smaller amount of available expansion work. Both the MT economization and ejector cycles would likely achieve higher maximum COP values than baseline, but the compressor was not able to reach a gas cooling pressure associated with a maximum COP for any of the cycles tested at the 28 °C condition. Therefore, higher COP benefits with the MT economization and ejector cycles at the 28 °C condition may be achievable with a larger compressor.

5. CONCLUSIONS

This paper presented an experimental analysis comparing four cycle architectures applied in a two-evaporator transcritical CO_2 refrigeration cycle with an approximate capacity of 8 kW. The assessed cycles were (1) no economization, (2) flash tank economization applied upstream of the MT evaporator, (3) ejector and MT economization, and (4) ejector, MT economization, and a pump upstream of the motive nozzle inlet. The comparison was conducted over a range of four ambient temperatures ranging from 14 °C to 28 °C. The gas cooler outlet pressure was varied at each ambient condition for each cycle in an effort to identify the gas cooling pressure that resulted in the maximum COP. The gas cooling pressure where the maximum COP occurred for each cycle decreased as ambient temperature decreased. Maximum COP benefits of 6% and 5% were achieved at the 19 °C ambient condition with the MT economization cycle and ejector cycle respectively. The pump was able to increase ejector efficiency, however, all tests utilizing the pump resulted in a lower COP than the ejector cycle without the pump due to the need to optimize both the pump and the ejector for this specific application. The combination of the pump and ejector offers potential for overall performance improvement, and a specific focus on the design of these components is in the future work.

Future work is to optimize both ejector and pump designs for the operating conditions and capacity of this test stand to increase the COP benefit of both cycles. Additionally, the first stage compressor needs to be optimized for booster operation, and the compressor performing the second and third stages of compression needs to have a larger capacity to achieve higher gas cooling pressures at high ambient conditions. A suction-to-liquid-line heat exchanger should also be considered at the outlet of the flash tank in order to provide sub-cooled liquid to facilitate a more accurate mass flow reading from a Coriolis-effect mass flow meter and at the outlet of the gas cooler to enable use of the pump at higher ambient temperature conditions.

ACKNOWLEDGEMENTS

The authors would like to thank the Bechtel Corporation for providing intellectual property, financial and technical support as well as the faculty and staff of the Ray W. Herrick Labs for financial and technical support.

REFERENCES

Bahman, A.M., Barta, R.B., Ziviani, D., Groll, E.A. 2021. CO2 Heat Pump: Fundamentals and Application, Wiley. Editor: Xin-Rung Zhang. Chapter: "Theoretical Analysis of CO_2 Expansion Process," https://doi.org/10.1002/9781118380055.ch5

Barta, R.B., Hugenroth, J.J., Groll, E.A., 2018. Modeling of S-RAM energy recovery compressor integration in a transcritical carbon dioxide cycle for application in multi-temperature refrigerated container systems, in: 13th IIR Gustav Lorentzen Conference. https://doi.org/10.18462/iir.gl.2018.1117

Elbel, S., Hrnjak, P., 2008. Experimental validation of a prototype ejector designed to reduce throttling losses encountered in transcritical R744 system operation. Int. J. Refrig. 31, 411–422.

Gay, N.H., 1931. Refrigerating System. US Pat. 1,836,318.

Gullo, P., Hafner, A., 2017. Thermodynamic Performance Assessment of a CO2 Supermarket Refrigeration System with Auxiliary Compression Economization by using Advanced Exergy Analysis. Int. J. Thermodyn 20, 220–227.

Gullo, P., Hafner, A., Banasiak, K., 2018. Transcritical R744 refrigeration systems for supermarket applications: Current status and future perspectives. Int. J. Refrig. 93, 269–310. https://doi.org/10.1016/j.ijrefrig.2018.07.001

Hafner, A., Försterling, S., Banasiak, K., 2014. Multi-ejector concept for R-744 supermarket refrigeration. Int. J. Refrig. 43, 1–13.

Haida, M., Banasiak, K., Smolka, J., Hafner, A., Eikevik, T.M., 2016. Experimental analysis of the R744 vapour compression rack equipped with the multi-ejector expansion work recovery module. Int. J. Refrig. 64, 93–107.

Karampour, M., Sawalha, S., 2018. State-of-the-art integrated CO2refrigeration system for supermarkets: A comparative analysis. Int. J. Refrig. 86. https://doi.org/10.1016/j.ijrefrig.2017.11.006

Kemper, G.A., Harper, G.F., Brown, G.A., 1996. Multiple Phase Ejector Refrigeration System. 3,277,660.

Kim, M.H., Pettersen, J., Bullard, C.W., 2004. Fundamental process and system design issues in CO2 vapor compression systems. Prog. Energy Combust. Sci. 30, 119–174. https://doi.org/10.1016/j.pecs.2003.09.002

Ladd, D., 2019a. Systems and methods for multi stage refrigeration. U.S. Pat. Number US 10,465,983 B2.

Ladd, D., 2019b. Systems and methods for multi stage refrigeration. U.S. Pat. Number US 10,514,202 B2.

Ladd, D., 2019c. Systems and methods for multi stage refrigeration. U.S. Pat. Number US 10,514,201 B2.

Ladd, D., 2018. Systems and Methods for Multi-Stage Refrigeration. U.S. Pat. Number US 2018 / 0231304 A1.

Lawrence, N., Elbel, S., Hrnjak, P.S., 2018. Design and validation of a transcritical CO2 mobile refrigerated container system for military applications, in: 13th IIR Gustav Lorentzen Conference on Natural Refrigerants. pp. 882–890.

Liu, F., Li, Y., Groll, E.A., 2012. Performance enhancement of CO2 air conditioner with a controllable ejector. Int. J. Refrig. 35, 1604–1616.

Lorentzen, G., 1994. Revival of carbon dioxide as a refrigerant. Int. J. Refrig. 17, 292–301. https://doi.org/10.1016/0140-7007(94)90059-0

Lucas, C., Koehler, J., 2012. Experimental investigation of the COP improvement of a refrigeration cycle by use of an ejector. Int. J. Refrig. 35, 1595–1603.

Minetto, S., Brignoli, R., Zilio, C., Marinetti, S., 2014. Experimental analysis of a new method for overfeeding multiple evaporators in refrigeration systems. Int. J. Refrig. 38, 1–9.

Newton, A.B., 1972. Capacity Control for Multiple-Phase Refrigeration Systems. US Pat. 3,670,519.

Taylor, B.N., Kuyatt, C.E., 1994. NIST Technical Note 1297 1994 Edition, Guidelines for Evaluating and Expressing the Uncertainty of NIST Measurement Results. Natl. Inst. Stand. Technol. 1–20.

Zhu, J., Elbel, S., 2018. Experimental investigation of a novel expansion device control mechanism: Vortex control of initially subcooled flashing R134a flow expanded through convergent-divergent nozzles. Int. J. Refrig. 85, 167–183.

NOMENCLATURE

d	Diameter	(mm)	LT	Low temperature
h	Specific enthalpy	(kJ kg^{-1})	mi	Ejector motive nozzle inlet
m	Mass	(kg)	motive	Ejector motive nozzle
$\dot{m}$	Mass flow rate	(kg s^{-1})	MT	Medium temperature
P	Pressure	(kPa, bar)	out	Outlet

$\dot{Q}$	Heat transfer rate	(kW)	si	Ejector suction nozzle inlet
s	Specific entropy	[kJ (kg-K)$^{-1}$]	suction	Ejector suction nozzle
T	Temperature	(°C, K)	X	Measured quantity
U	Uncertainty	(various)	Y	Calculated quantity
$\dot{V}$	Volumetric flow rate	(m^3 hr^{-1})	1,2,3…	State points
w	Entrainment ratio	(-)		
$\dot{W}$	Power	(kW)	**Acronyms**	
x	Quality	(-)	COP	Coefficient of Performance
			CO_2	Carbon Dioxide
Greek symbols			EG	Ethylene Glycol
η	Efficiency	(-, %)	EXV	Electronic Expansion Valve
			FS	Full Scale
Subscript			GWP	Global Warming Potential
comp	Compressor		HFC	Hydrofluorocarbon
cool	Cooling capacity		HP	High Pressure
d	Ejector diffuser outlet		LP	Low Pressure
EG	Ethylene-glycol		LT	Low Temperature
GC	Gas cooler		MT	Medium Temperature
HP	High pressure		P&ID	Piping and Instrumentation Diagram
i	Iteration counter		RDG	Reading
LP	Low pressure		VFD	Variable Frequency Drive